Int. J. Heat Mass Transfer. Vol. 24, No. 4, pp. 727–737, 1981
Printed in Great Britain

0017–9310/81/040727–11$02.00/0
Pergamon Press Ltd

NATURAL CONVECTION IN AN INCLINED CIRCULAR CYLINDRICAL ANNULUS HEATED AND COOLED ON ITS END PLATES

HIROYUKI OZOE and TSUTOMU SHIBATA
Department of Industrial and Mechanical Engineering,
Okayama University, Okayama, Japan
and
STUART W. CHURCHILL
Department of Chemical Engineering, University of Pennsylvania, Philadelphia, PA, U.S.A.

(*Received* 20 *February* 1980)

Abstract — Natural convection in an inclined annular space heated and cooled on the end plates and thermally insulated on the concentric cylinder walls was studied experimentally and theoretically. As the heated surface was inclined from the lower horizontal position to an upper horizontal position, the mean Nusselt number at first decreased, then increased and finally decreased to unity as the mode of circulation switched from a symmetrical array of roll cells to distorted and oblique roll cells to a single circulation. The flow pattern is portrayed with streaklines computed numerically using a three-dimensional model and also with photographs.

NOMENCLATURE

A, heat transfer surface [m^2];
g, acceleration due to gravity [$m\,s^{-2}$];
k, thermal conductivity of fluid [$W\,m^{-1}\,K^{-1}$];
l, axial length of annulus [m];
Nu, mean Nusselt number $= Q_{net}l/kA(T_h - T_c)$;
Pr, Prandtl number $= \nu/\alpha$;
Q, heat flux [W];
R, dimensionless radial coordinate $= r/l$;
r, radial coordinate [m];
r_1, inner radius of annulus [m];
r_2, outer radius of annulus [m];
Ra, Rayleigh number $= g\beta(T_h - T_c)l^3/\alpha\nu$;
T, temperature [K];
$\bar{T}$, dimensionless temperature $= (T - T_0)/(T_h - T_c)$;
t, time [s];
U, dimensionless radial component of velocity $= ul/\alpha$;
u, radial component of velocity [$m\,s^{-1}$];
V, dimensionless angular component of velocity $= vl/\alpha$;
v, angular component of velocity [$m\,s^{-1}$];
W, dimensionless axial component of velocity $= wl/\alpha$;
w, axial component of velocity [$m\,s^{-1}$];
Z, dimensionless axial coordinate $= z/l$;
z, axial coordinate of annulus [m].

Greek symbols

α, thermal diffusivity of fluid [$m^2\,s^{-1}$];
β, volumetric coefficient of expansion with temperature [K^{-1}];
θ, angular coordinate [rad];
ν, kinematic viscosity of fluid [$m^2\,s^{-1}$];
ρ, density of fluid [$kg\,m^{-3}$];
τ, dimensionless time $= t\alpha/l^2$;
ψ, dimensionless vector potential;
Ω, dimensionless vorticity vector;
ϕ, angle of inclination of the heated plate from lower horizontal position [rad].

Subscripts

0, value at mean temperature, $T_0 = (T_h + T_c)/2$;
1, vector component in a radial direction;
2, vector component in a circumferential direction;
3, vector component in an axial direction;
c, value at cooled plate;
h, value at heated plate;
net, net heat flux;
total, total heat flux.

1. INTRODUCTION

NATURAL convection in an annular space bounded by two concentric cylinders and two plates normal to the common axis of the cylinders has been studied previously only for vertical and horizontal orientations of the axis. For the horizontal orientation with uniform heat flux densities or uniform temperatures on the inner and outer curved surfaces, the fluid motion approaches two-dimensionality as the length to diameter ratio increases. Hence this geometrical arrangement has received primary attention both theoretically and experimentally. (See, for example, Kuehn and

Goldstein [1] and Seki, Fukusako and Nakaoka [2].) For the vertical orientation of the axis with heating and cooling of the flat surfaces, the motion is strongly three-dimensional. Prior work for this geometrical arrangement is very limited. Stork and Müller [3] photographed the flow pattern, analyzed the stability of different modes of circulation and noted the number of roll cells. Ozoe, Okamoto and Churchill [4] photographed particle-paths of short duration in radial and horizontal planes. They also developed a three-dimensional numerical solution using finite-difference calculations. They found that the stable motion consisted of a single ring of identical roll cells with radial axes. The number of these cells was equal to the even integer nearest to the average circumference divided by the height. The particle paths within a roll cell all have the form of a double concentric helix and are confined to one or the other half of the roll cell.

This paper presents the results of an experimental and theoretical investigation of natural convection in an inclined annular region heated on one plane surface and cooled on the other.

2. EXPERIMENTAL APPARATUS AND METHODS

The experimental apparatus, as shown in Fig. 1, is similar to that used by Ozoe, Okamoto and Churchill [4]. The test region was formed by Plexiglas cylinders 20 mm long and 50 mm and 100 mm in diameter with copper end-plates. The gaskets between the plates and the cylinders resulted in a 20.9 mm distance between the hot and cold plates. The lower plate was heated with nichrome wire backed up with asbestos and wood as insulation. The upper plate was cooled with water from a bath at constant temperature. The temperature was measured at a number of points on both plates. The annulus was insulated on both external surfaces with glass fibers. The room in which the experiments were carried out was maintained at the temperature of the cooled plate. Heat losses were estimated by measuring the wattage with the hot plate on top and subtracting the rate of conduction through the liquid. The losses were correlated linearly with the temperature difference. Glycerol with dispersed flakes of aluminum was used to photograph the mode of flow, but silicone oil was used for the experiments in which the heat flux was measured. For photographic purposes, the top cooling jacket was replaced with a glass box through which cooling water from a constant temperature bath was circulated. Most of the flow visualization experiments were performed for the annular region with an axial length of 26 mm.

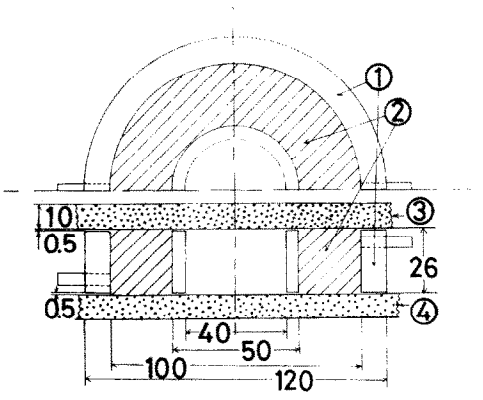

FIG. 1. Top and front view of an annular space heated on one end plate, cooled on the other end and thermally insulated on the inner and outer circular walls. (Dimensions in mm.) 1 transparent Plexiglas; 2 experimental fluid; 3 cooled plate of either copper or glass; 4 heated plate of copper.

3. EXPERIMENTAL RESULTS

The heat transfer rate was first measured with the annular axis in the vertical direction and the heated surface at the bottom. The results are shown in Fig. 2. The two runs agree fairly well, and, owing to the vertical drag of the inner and outer cylinder walls, give a definitely smaller Nusselt number at small Rayleigh number than the curve of Silveston [5] for a wide horizontal fluid layer. The rate of heat transfer for silicone oil in the annulus is plotted in Fig. 3 vs the angle of inclination. These experiments were for a total heat input of 8.96 W. A minimum in the heat flux appears to occur at about $\pi/9$–$\pi/6$ rad of inclination of the heated plate from the lower horizontal position and a maximum at about $\pi/3$ rad. These characteristics are quite similar to those observed for natural convection in an inclined rectangular box [6].

The mode of flow as photographed through a transparent glass plate has not previously been clearly identified as a function of an angle of inclination. When the heated plate is horizontal and at the bottom, the mode of circulation is a series of roll cells with their axes in the radial direction as previously reported by Ozoe, Okamoto and Churchill [4]. For this orientation and geometry, the total number of roll cells in the present enclosure is ten as indicated in Fig. 4.

At $\pi/60$ rad of inclination, the number of roll cells decreased from ten to eight and this mode of circulation persisted even at $\pi/36$ rad of inclination as seen in Fig. 5.

At $7\pi/180$ rad of inclination, the mode of circulation became toroidal as indicated in Fig. 6, but some trace of the roll cells is still apparent. Photographs were not obtained between this angle and $\pi/2$ rad but one photograph is available for an annulus with an axial length of 20.9 mm rather than 26 mm, as shown in Fig. 7. This picture reveals the mode of circulation at an intermediate angle of inclination of $34\pi/180$ rad. The toroidal pattern is modified by the development of a flow up along the heated plate and down along the cooled plate on the left hand side of annular space where a wide gap is available to the fluid.

As seen in Fig. 8 at $\pi/2$ rad of inclination, the flow near the vertical cold wall is downward over a large

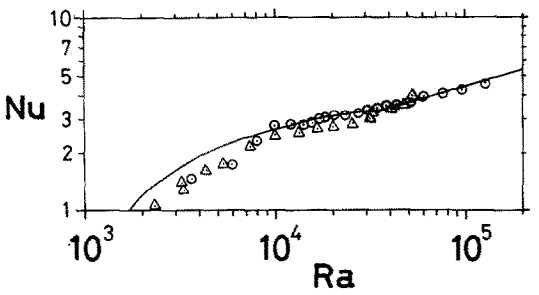

FIG. 2. Experimental rates of heat transfer for $\phi = 0$, $r_1 = 25\,\text{mm}$, $r_2 = 50\,\text{mm}$ and $l = 20.9\,\text{mm}$. Silicone oil ($5 \times 10^{-4}\,\text{m}^2\,\text{s}^{-1}$ at 298.1 K). The solid line represents graphical correlation of Silveston [5] for a wide horizontal layer of fluid. ○ run 1; △ run 2.

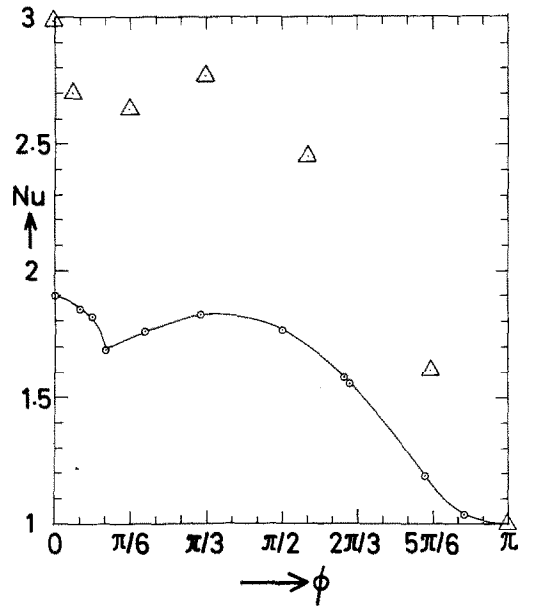

FIG. 3. Experimental and theoretical rates of heat transfer in the inclined annular enclosure of Fig. 1. △ experimental points for $Ra = 38\,100$–$28\,500$, $Pr = 2580$–2700 and $Q_{\text{total}} = 8.96\,\text{W}$. –○– computed values (extrapolated to zero grid size) for $Ra = 6000$, $Pr = 10$, $r_1/l = 0.5$, $r_2/l = 1.5$.

region and the top side of the inner cylinder becomes a stagnation front. On the other hand, the lower side of the inner cylinder shows a wake-like behavior. Figure 9, at 5 mm from the heated plate, shows a similar pattern. The flow is now upward and the lower side of the inner cylinder becomes a stagnation front for the upward flow.

These photographs provide a test for the numerical solution described below.

4. MATHEMATICAL MODEL

Natural convection in the annular space of Fig. 10 is described by the equations for the conservation of mass, momentum and energy in the r-, θ- and z-directions, simplified in accordance with the Boussinesq assumption. The components of gravity in the r-, θ- and z-directions are $-g\sin\phi\cos\theta$, $g\sin\phi\sin\theta$ and $g\cos\theta$, respectively. Taking cross derivatives of the momentum equations and subtracting out the pressure terms, introducing the vorticity and dedimensionalizing then yields the following dimensionless vorticity and energy equations

$$\frac{1}{Pr}\left(\frac{\partial\Omega_1}{\partial\tau} + U\frac{\partial\Omega_1}{\partial R} + \frac{V}{R}\frac{\partial\Omega_1}{\partial\theta} + W\frac{\partial\Omega_1}{\partial Z} - \Omega_1\frac{\partial U}{\partial R} - \frac{\Omega_2}{R}\frac{\partial U}{\partial\theta} - \Omega_3\frac{\partial U}{\partial Z}\right) = \frac{\partial^2\Omega_1}{\partial R^2} + \frac{1}{R}\frac{\partial\Omega_1}{\partial R} - \frac{\Omega_1}{R^2} - \frac{2}{R^2}\frac{\partial\Omega_2}{\partial\theta} + \frac{1}{R^2}\frac{\partial^2\Omega_1}{\partial\theta^2} + \frac{\partial^2\Omega_1}{\partial Z^2} + Ra\left(\frac{\partial\bar{T}}{\partial Z}\sin\phi\sin\theta - \frac{1}{R}\frac{\partial\bar{T}}{\partial\theta}\cos\phi\right) \quad (1)$$

$$\frac{1}{Pr}\left(\frac{\partial\Omega_2}{\partial\tau} + U\frac{\partial\Omega_2}{\partial R} + \frac{V}{R}\frac{\partial\Omega_2}{\partial\theta} + W\frac{\partial\Omega_2}{\partial Z} - \Omega_1\frac{\partial V}{\partial R} - \frac{\Omega_2}{R}\frac{\partial V}{\partial\theta} - \Omega_3\frac{\partial V}{\partial Z} + \frac{V\Omega_1 - U\Omega_2}{R}\right) = \frac{\partial^2\Omega_2}{\partial R^2} + \frac{1}{R}\frac{\partial\Omega_2}{\partial R} - \frac{\Omega_2}{R^2} + \frac{1}{R^2}\frac{\partial^2\Omega_2}{\partial\theta^2} + \frac{2}{R^2}\frac{\partial\Omega_1}{\partial\theta} + \frac{\partial^2\Omega_2}{\partial Z^2} + Ra\left(\frac{\partial\bar{T}}{\partial R}\cos\phi + \frac{\partial\bar{T}}{\partial Z}\sin\phi\cos\theta\right) \quad (2)$$

$$\frac{1}{Pr}\left(\frac{\partial\Omega_3}{\partial\tau} + U\frac{\partial\Omega_3}{\partial R} + \frac{V}{R}\frac{\partial\Omega_3}{\partial\theta} + W\frac{\partial\Omega_3}{\partial Z} - \Omega_1\frac{\partial W}{\partial R} - \frac{\Omega_2}{R}\frac{\partial W}{\partial\theta} - \Omega_3\frac{\partial W}{\partial Z}\right) = \frac{\partial^2\Omega_3}{\partial R^2} + \frac{1}{R}\frac{\partial\Omega_3}{\partial R} + \frac{1}{R^2}\frac{\partial^2\Omega_3}{\partial\theta^2} + \frac{\partial^2\Omega_3}{\partial Z^2} + Ra\left(-\frac{1}{R}\frac{\partial\bar{T}}{\partial\theta}\sin\phi\cos\theta - \frac{1}{R}\frac{\partial(R\bar{T})}{\partial R}\sin\phi\sin\theta\right) \quad (3)$$

and

$$\frac{\partial\bar{T}}{\partial\tau} + U\frac{\partial\bar{T}}{\partial R} + \frac{V}{R}\frac{\partial\bar{T}}{\partial\theta} + W\frac{\partial\bar{T}}{\partial Z} = \frac{\partial^2\bar{T}}{\partial R^2} + \frac{1}{R}\frac{\partial\bar{T}}{\partial R} + \frac{1}{R^2}\frac{\partial^2\bar{T}}{\partial\theta^2} + \frac{\partial^2\bar{T}}{\partial Z^2}. \quad (4)$$

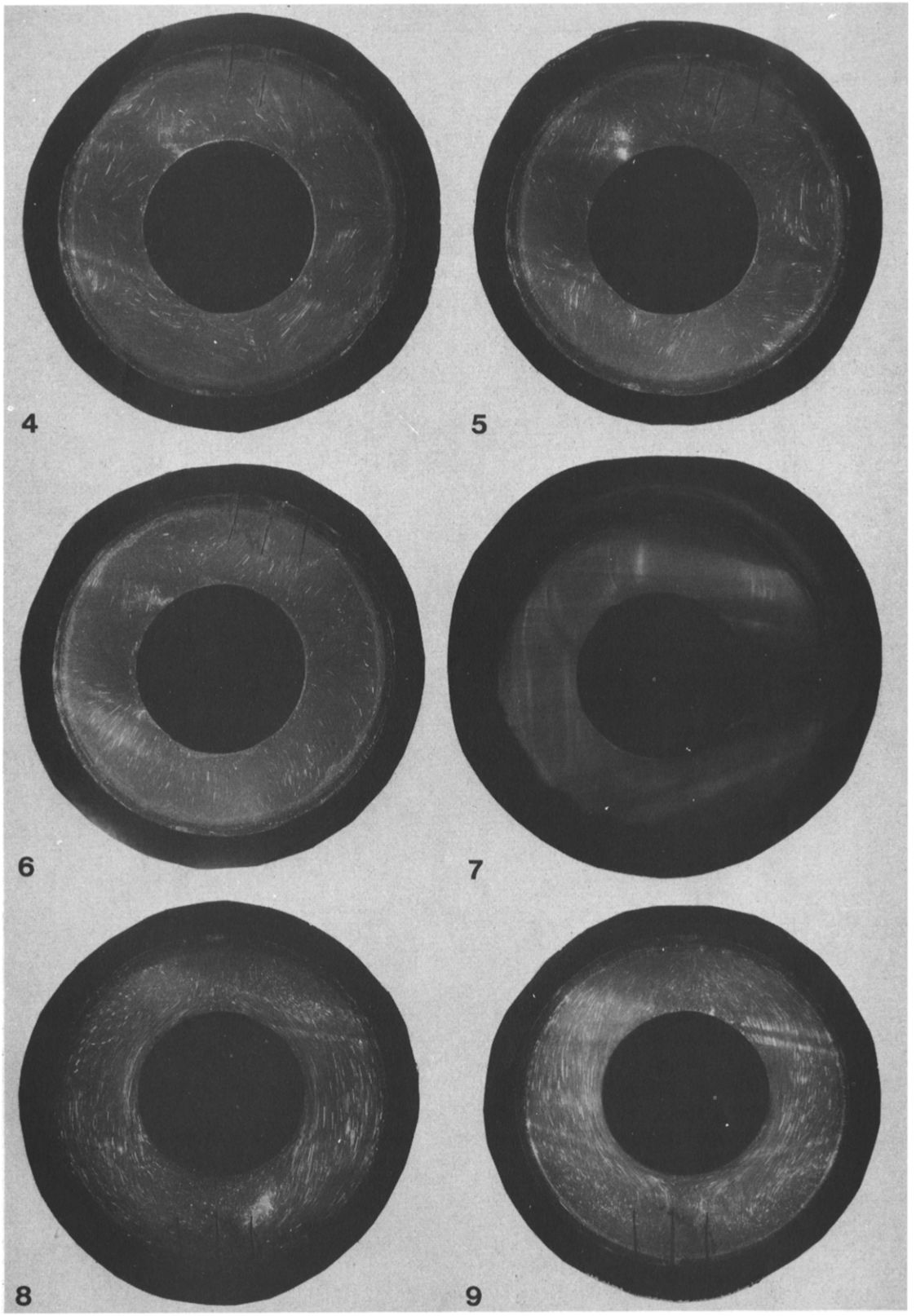

FIGS. 4–9

FIG. 4. Streakline photograph. End view for $\phi = 0$ in glycerol with $r_1 = 25$ mm, $r_2 = 50$ mm, $l = 26$ mm, $Ra = 48\,000$, $Pr = 2700$ and $Q_{total} = 9.4$ W. Photographed plane is 5 mm from the cooled plate with an exposure time of 15 s. FIG. 5. Streakline photograph. End view for $\phi = \pi/36$ rad with $Ra = 46\,000$, $Pr = 2800$ and $Q_{total} = 9.4$ W. Otherwise the conditions are the same as for Fig. 4. FIG. 6. Streakline photograph. End view for $\phi = 7\pi/180$ rad, $Ra = 48\,000$, $Pr = 2700$ and $Q_{total} = 9.4$ W. Otherwise the conditions are the same as for Fig. 4. FIG. 7. Streakline photograph. End view for $\phi = 34\pi/180$ rad, $r_1 = 25$ mm, $r_2 = 50$ mm, $l = 20.9$ mm, $Ra = 35\,000$, $Pr = 2900$ and $Q_{total} = 8.96$ W. Photographed plane is 5 mm from the heated plate. FIG. 8. Streakline photograph. End view for $\phi = \pi/2$ rad, $Ra = 67\,800$, $Pr = 2400$ and $Q_{total} = 9.4$ W. Photographed plane is 5 mm from the cooled plate. Otherwise the conditions are the same as in Fig. 4. FIG. 9. Streakline photograph. End view for $\phi = \pi/2$ rad, $Ra = 67\,800$, $Pr = 2400$ and $Q_{total} = 9.4$ W. Photographed plane is 5 mm from the heated plate. Otherwise the conditions are the same as in Fig. 4.

The components of dimensionless vorticity are here

$$\Omega_1 = \frac{1}{R}\frac{\partial W}{\partial \theta} - \frac{\partial V}{\partial Z} \tag{5}$$

$$\Omega_2 = \frac{\partial U}{\partial Z} - \frac{\partial W}{\partial R} \tag{6}$$

and

$$\Omega_3 = \frac{1}{R}\frac{\partial (RV)}{\partial R} - \frac{1}{R}\frac{\partial U}{\partial \theta}. \tag{7}$$

The components of the dimensionless velocity are related to the components of the dimensionless vector potential as follows:

$$U = \frac{1}{R}\frac{\partial \psi_3}{\partial \theta} - \frac{\partial \psi_2}{\partial Z} \tag{8}$$

$$V = \frac{\partial \psi_1}{\partial Z} - \frac{\partial \psi_3}{\partial R} \tag{9}$$

and

$$W = \frac{1}{R}\frac{\partial (R\psi_2)}{\partial R} - \frac{1}{R}\frac{\partial \psi_1}{\partial \theta}. \tag{10}$$

This vector potential is assumed to be solenoidal, i.e.

$$\frac{1}{R}\frac{\partial (R\psi_1)}{\partial R} + \frac{1}{R}\frac{\partial (\psi_2)}{\partial \theta} + \frac{\partial (\psi_3)}{\partial Z} = 0. \tag{11}$$

It follows from equations (5)–(7) and (8)–(11) that

$$\Omega_3 = -\frac{\partial^2 \psi_3}{\partial R^2} - \frac{1}{R}\frac{\partial \psi_3}{\partial R} - \frac{1}{R^2}\frac{\partial^2 \psi_3}{\partial \theta^2} - \frac{\partial^2 \psi_3}{\partial Z^2} \tag{12}$$

$$\Omega_1 = -\frac{\partial^2 \psi_1}{\partial R^2} - \frac{1}{R^2}\frac{\partial (R\psi_1)}{\partial R} - \frac{2}{R}\frac{\partial \psi_1}{\partial R} - \frac{1}{R^2}\frac{\partial^2 \psi_1}{\partial \theta^2} - \frac{\partial^2 \psi_1}{\partial Z^2} - \frac{2}{R}\frac{\partial \psi_3}{\partial Z} \tag{13}$$

and

$$\Omega_2 = -\frac{\partial^2 \psi_2}{\partial R^2} + \frac{\psi_2}{R^2} - \frac{1}{R}\frac{\partial \psi_2}{\partial R} - \frac{1}{R^2}\frac{\partial^2 \psi_2}{\partial \theta^2} - \frac{2}{R^2}\frac{\partial \psi_1}{\partial \theta} - \frac{\partial^2 \psi_2}{\partial Z^2}. \tag{14}$$

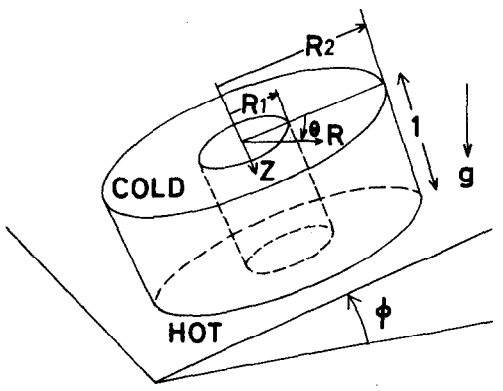

FIG. 10. Dimensionless coordinates for an inclined annular space.

Thus the components of the dimensionless vorticity are related to those of the dimensionless vector potential and vice versa.

Boundary conditions analogous to those used by Ozoe, Okamoto and Churchill [4] are at $R = R_1, R_2$

$$\frac{\partial (R\psi_1)}{\partial R} = \psi_2 = \psi_3 = U = V = W = \frac{\partial T}{\partial R} = \Omega_1 = 0$$

$$\Omega_2 = -\frac{\partial W}{\partial R} \quad \text{and} \quad \Omega_3 = \frac{1}{R}\frac{\partial (RV)}{\partial R}$$

at $\theta = 0, \pi$

$$\psi_1 = \frac{\partial \psi_2}{\partial \theta} = \psi_3 = \Omega_1 = \Omega_3 = \frac{\partial T}{\partial \theta} = \frac{\partial U}{\partial \theta} = V = \frac{\partial W}{\partial \theta} = 0 \quad \text{and} \quad \frac{\partial \Omega_2}{\partial \theta} = 0$$

and, at $Z = 0, 1$

$$\psi_1 = \psi_2 = \frac{\partial \psi_3}{\partial Z} = \Omega_3 = U = V = W = 0$$

$$\Omega_1 = -\frac{\partial V}{\partial Z}, \quad \Omega_2 = \frac{\partial U}{\partial Z} \quad \text{and} \quad T = \mp 0.5.$$

These equations were approximated by finite-difference equations and solved by the general A.D.I. method of Brian [7]. The steady-state was computed transiently starting from either the static-state or another steady- or transient-state. The energy equation was first solved for a time-step, then the three vorticity equations. The vector potential at each grid point was next computed from the known vorticity. In this case, equation (12) was first solved for ψ_3 from Ω_3, then equation (13) was solved for ψ_1, using the updated value of ψ_3. Equation (14) was then solved for ψ_2 using the updated value of ψ_1.

5. NUMERICAL RESULTS AND FLOW PATTERN

The computations were carried out for only one half of the annular space since symmetry in terms of the central vertical plane was expected. Ten grid points were used in both the radial and vertical directions and thirty in the azimuthal direction. The height of the annular cylinder was taken to be unity, the radius of the inner cylinder to be half of the height and the radius of the outer cylinder to be 1.5 times the height. The average circumference was $2\pi(0.5 + 1.5)/2 = 6.28$. Six roll cells are stable for this geometry according to the previously mentioned rule of thumb of Ozoe, Okamoto and Churchill [4]. This particular geometry was chosen to minimize the demands on the computer memory and computing time at the expense of some differences from the experimental case.

The temperatures at the upper and lower plates were set at -0.5 and 0.5, respectively. The inner and outer cylindrical walls were considered to be perfectly insulated and rigid. The parameters were $Ra = 6000$, $Pr = 10$ and various angles of inclination. For the

horizontal case, an initial temperature shock was introduced within the fluid to initiate three roll cells and thereby reduce the transient computing time.

This value of Pr is less than those of the experiments but the effect of Pr is known to be negligible for $Pr \gg 1$ [8]. A higher value in the computations would have increased the computational time without changing the results significantly. The value of Ra used in the computations is also much smaller than in the experiments. The lower value leads to a lower rate of circulation and heat transfer but the pattern of circulation and the relative dependence on the angle of inclination is known from previous work [9] to be essentially independent of Ra. The lower value was chosen because the computational time would have been excessive for the experimental conditions. On the other hand, the experiments at $Ra = 6000$ or so requires a smaller total rate of heating by one order than the current rate and the measurement of such a low rate becomes inaccurate.

The computed results are summarized in Fig. 3, in which the average Nusselt number is plotted vs angle of inclination. The results are in qualitative agreement with the experiments but differ quantitatively owing to the different parametric conditions. The heat transfer rate initially decreases with the angle of inclination due to the skewed and reverse flow. At $\pi/9$ rad of inclination, the Nusselt number goes through a local minimum. At higher angles of inclination the Nusselt number attains a maximum at about $\pi/3$ rad, then decreases to unity for pure conduction at π rad of inclination. This behavior can be rationalized by reference to the following streakline plots.

The steady-state velocity profile was used to compute the streaklines. Various starting points were chosen and tracers were advanced for a thousand time steps with $\Delta\tau = 0.002$. Figure 11 is a top view for the horizontal orientation with six different tracers. The three roll cells are made up of half cells separated at about the middle radius. A coaxial double helical movement is observed just as for rectangular enclosures [6].

When the annular space was inclined slightly ($\pi/12$ rad), one of the three roll cells shrank in size and other two strengthened as shown in the top view of Fig. 12 and the perspective view of Fig. 13. The inner roll cell would disappear for a slightly greater increase in inclination.

At $\pi/10$ rad of inclination, the transient calculation did not converge in 880 time steps and was abandoned. Short-time streaklines for this case are shown in Fig. 14 at $z = 0.2$ (near the cold wall). This graph suggests the presence of two main roll cells with a small complicated intermediate circulation. Curve 4 in Fig. 15 shows the transient response of the Nusselt number from $\phi = \pi/18$ to $\pi/9$ rad of inclination. The Nusselt number goes through a minimum as the mode of circulation changes from three roll cells to a single roll cell. A similar transient behaviour was observed for a rectangular enclosure [10], for which the roll cell rotating against the buoyant force disappeared and that rotating along the heated plate prevailed. The transient response for other conditions is also shown in Fig. 15.

The two streak lines in Fig. 16 for an angle of inclination of $\pi/9$ rad reveal a toroidal circulation near the plane of symmetry with an axis in the circumferential direction. In the intermediate region from $\phi = \pi/4$ to $3\pi/4$ rad, the circulation has a horizontal and radial axis rather than a circumferential one, as indicated in Fig. 17 for two additional starting points. The streakline starting from the central height near the outer cylinder wall indicates a possible local oscillation. This flow pattern can also be described by short multiple streaklines as shown in Fig. 18, for which all of the starting points are in the $Z = 0.8$ plane. This mode of flow at $\pi/9$ rad of inclination appears to correspond to the photograph of Fig. 7 at $34\pi/180$ rad. The difference in the characteristic angle is due to the difference in the aspect ratios.

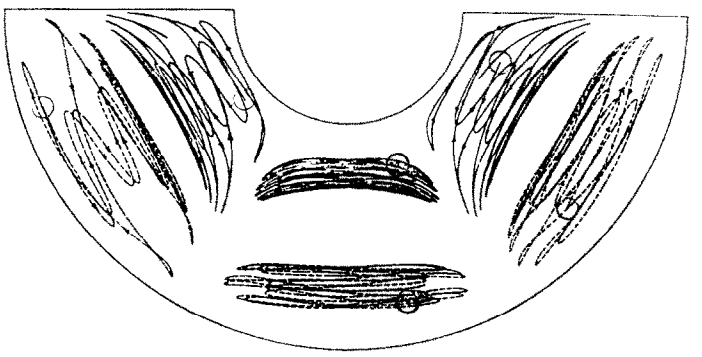

FIG. 11. Top view of streakines for $\phi = 0$, $Ra = 6000$, $Pr = 10$, $\Delta R = \Delta Z = 0.1$ and $\Delta\theta = \pi/30$ rad. Elapsed time, $\tau = 2$. Starting points are indicated by open circles and their locations in (R, θ, Z) coordinates are: (0.7, $\pi/10$, 0.4), (1.3, $7\pi/30$, 0.6), (0.7, $2\pi/5$, 0.2), (1.3, $13\pi/30$, 0.2), (0.6, $23\pi/30$, 0.3) and (1.4, $9\pi/10$, 0.7).

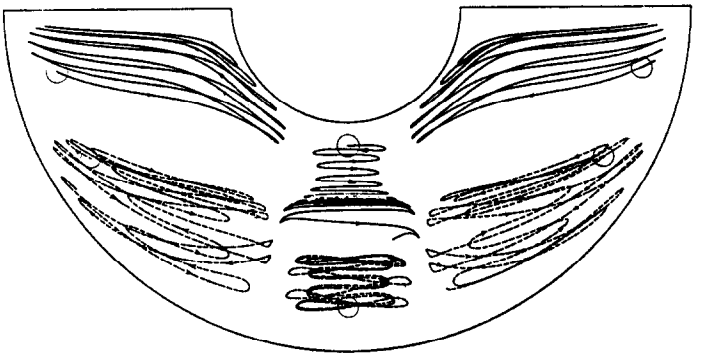

FIG. 12. Streaklines in an annular space inclined at $\phi = \pi/12$ rad. Otherwise conditions are the same as in Fig. 11. Starting points are: $(1.3, \pi/15, 0.8)$, $(1.3, \pi/6, 0.2)$, $(0.6, \pi/2, 0.2)$, $(1.3, \pi/2, 0.2)$, $(1.3, 14\pi/15, 0.8)$ and $(1.3, 5\pi/6, 0.2)$.

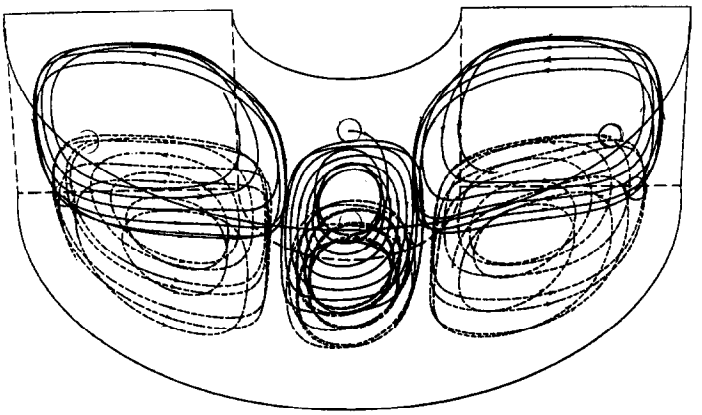

FIG. 13. Perspective view of streaklines of Fig. 12. Eye point is $(16, \pi/2, -12)$.

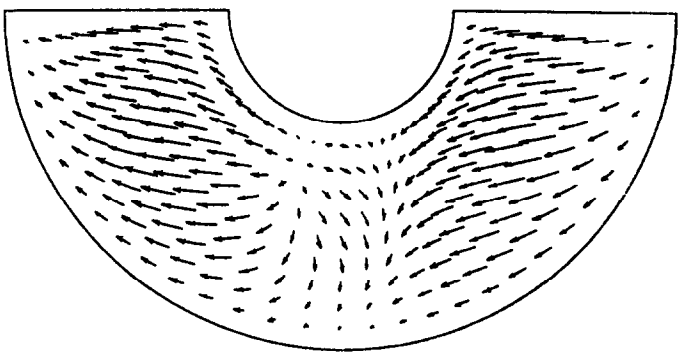

FIG. 14. Short-time, multiple streaklines for $\phi = \pi/10$ rad. Starting points are the grid points on the $Z = 0.2$ plane. Rlapsed time, $\tau = 0.009$.

At an inclination of $\pi/2$ rad, i.e. for a horizontal axis, the basic circulation is along the cold and hot plate as seen in Fig. 19. Even in this case, the small spiral in the central region and the big spiral in the outer region can be observed to come back to the inner cylinder wall area. A small spiral movement exists at this inclination, as indicated in Fig. 20. This secondary vortex apparently occurs because the inner cylinder wall acts as a barrier to the main circulation.

At the higher angles of inclination, for example, at 2 rad, as seen in Fig. 21, a similar mode of circulation was also observed. Even at this angle of inclination, a tracer started near the outer wall and midway between the heated and cooled plates rotates in quite a limited area.

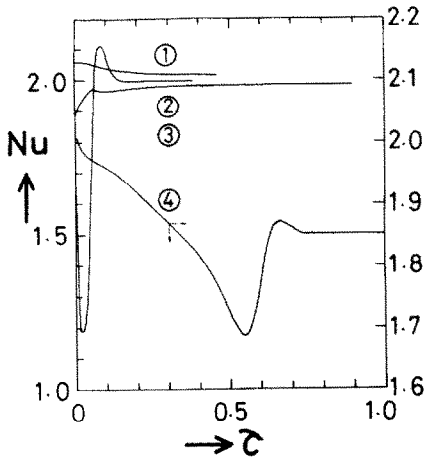

FIG. 15. Computed transient response of the Nusselt number after a change of angle of inclination: curve 1, for a final steady-state of $\phi = \pi/18$ rad, curve 2, for a final steady-state of $\phi = 1$ rad, curve 3, for a final steady-state of $\phi = \pi/12$ rad, curve 4, for a final steady-state of $\phi = \pi/9$ rad.

Short-time multiple streaklines started in the $Z = 0.2$ plane near the cooled wall are drawn in Fig. 22 for an inclination of $\pi/2$ rad. This streakline sketch agrees quite well with the photograph of Fig. 8 which was taken at 5 mm from the cooled wall in an annulus with an axial length of 26 mm.

From this series of streak lines, we can conclude and predict that laminar natural convection in such enclosed geometries consists of a pair of roll cells made up of double helical particle paths. Though the computations were only for $Ra = 6000$ and $Pr = 10$, similar behaviour would be expected for other related conditions and aspect ratios.

SUMMARY

At small angles of inclination, the rate of heat transfer in an annular space heated and cooled on the end plates decreases as the angle of inclination of the heated plate increases and the roll cells which rotate against the buoyant force shrink in size. At slightly larger angles, such as $\pi/36$ rad, the number of roll cells decreases and the remaining roll cells degrade in shape. This change is accompanied by a continued decrease in the rate of heat transfer. At $\pi/9$–$\pi/6$ rad, depending on the aspect ratio of the annular space, the roll cell mode changes to a circulating flow rising along the hot plate and descending along the cold plate. A minimum in the heat flux accompanies this change in the mode of circulation. For a further inclination, the rate of heat transfer increases and goes through a maximum at about $\pi/3$ rad and then decreases to the conduction state at $\phi = \pi$, corresponding to heating from above. Near the critical angle for the change in mode of circulation a toroidal mode is observed. For all angles of inclination, the circulation is made up of pairs of streaklines which trace out a closed concentric helix.

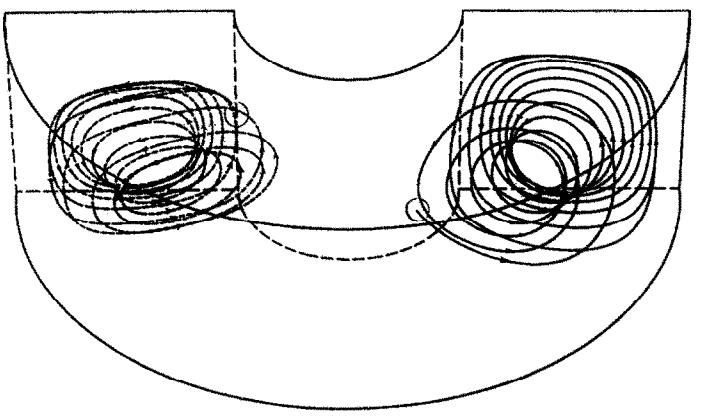

FIG. 16. Perspective view of two streaklines for $\phi = \pi/9$ rad. Eye point is $(16, \pi/2, -12)$. Elapsed time, $\tau = 2$. Starting points are $(0.6, \pi/3, 0.7)$ and $(0.6, 4\pi/5, 0.3)$.

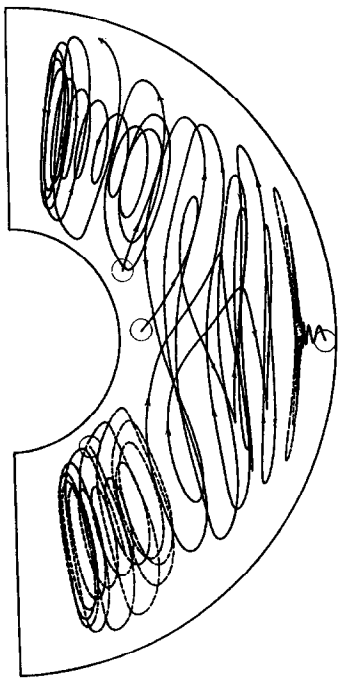

FIG. 17. Top view of four streaklines for $\phi = \pi/9$ rad. Elapsed time, $\tau = 2$. Starting points are (0.6, $\pi/3$, 0.7), (0.6, $87\pi/180$, 0.55), (0.6, $4\pi/5$, 0.3), and (1.45, $91.2\pi/180$, 0.52).

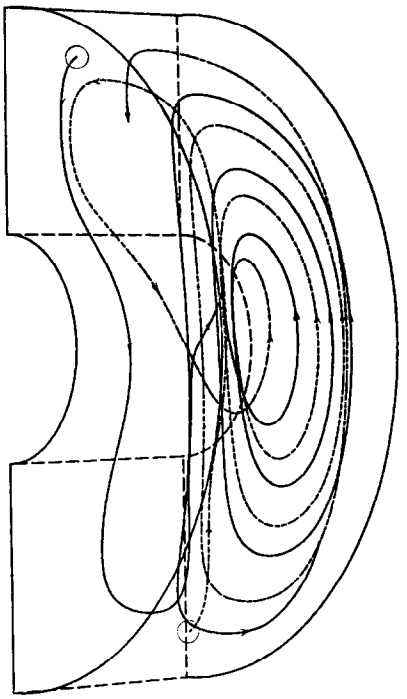

FIG. 19. Perspective view of streaklines for $\phi = \pi/2$ rad (horizontal axis). The cooled plate is on the near side. Elapsed time, $\tau = 2$. Eye point is (16, $\pi/2$, -12). Starting points are (1.3, $\pi/15$, 0.2) and (1.3, $14\pi/15$, 0.8).

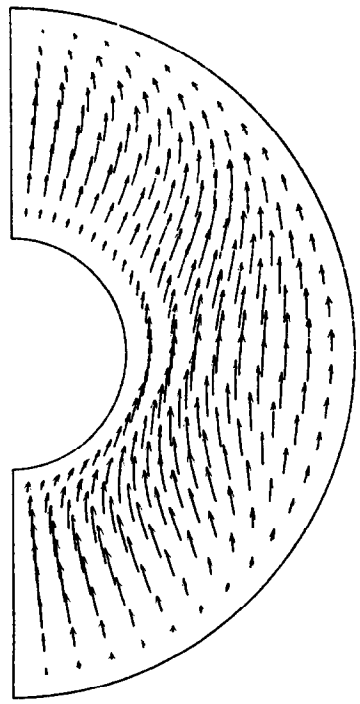

FIG. 18. Top view of multiple streaklines for $\phi = \pi/9$ rad. Elapsed time, $\tau = 0.009$. Starting points are the grid points on the $Z = 0.8$ plane.

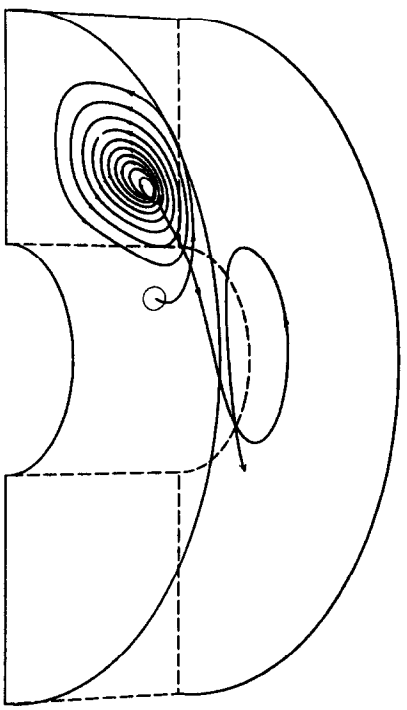

FIG. 20. Perspective view of streaklines for $\phi = \pi/2$ rad (horizontal axis). Elapsed time, $\tau = 2$. Eye point is (16, $\pi/2$, -12). Starting point is (0.52, $\pi/3$, 0.5).

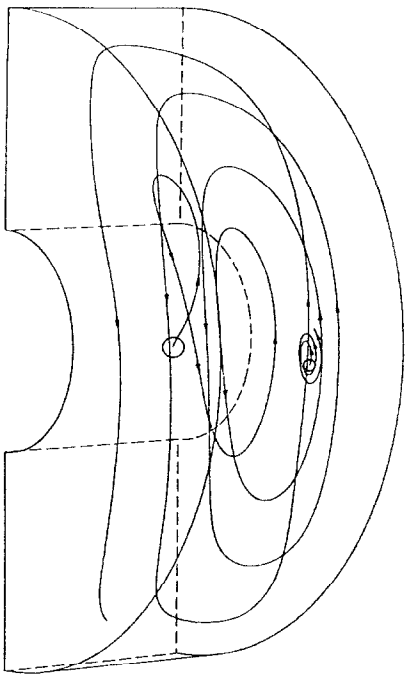

FIG. 21. Perspective view of streaklines for $\phi = 2$ rad. Elapsed time, $\tau = 2$. Eye point is (16.07, $84.64\pi/180$, -12). Starting points are (0.55, $91.8\pi/180$, 0.52) and (1.45, $91.8\pi/180$, 0.52).

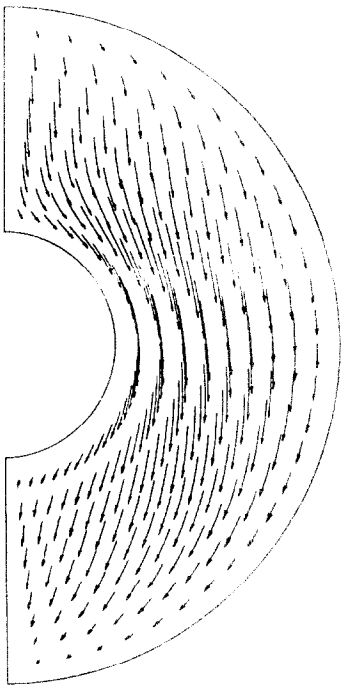

FIG. 22. Top view of multiple streaklines for $\phi = \pi/2$ rad (horizontal axis). Starting points are grid points on the $Z = 0.2$ plane near the cooled plate. Elapsed time, $\tau = 0.009$.

Acknowledgements — This work was made possible in part by the U.S.–Japan cooperative joint research project supported by the Japan Society for the Promotion of Science and the U.S. National Science Foundation. The computational work was carried out on the Acos 700 at Okayama University and at the Computer Center of the Department of Physics of the University of Pennsylvania. H. Kotani, K. Nagao and H. Nakashima assisted through their undergraduate thesis work. The encouragement of Professor Hayatoshi Sayama, Okayama University, is greatly appreciated.

REFERENCES

1. T. H. Kuehn and R. J. Goldstein, An experimental study of natural convection heat transfer in concentric and eccentric horizontal cylindrical annuli. *J. Heat Transfer* **100,** 635–640 (1978).
2. N. Seki, S. Fukusako and M. Nakaoka, An analysis of free convective heat transfer with density inversion of water between two horizontal concentric cylinders, *J. Heat Transfer* **98,** 670–672 (1976).
3. K. Stork and U. Müller, Convection in boxes: An experimental investigation in vertical cylinders and annuli, *J. Fluid Mech.* **71,** 231–240 (1975).
4. H. Ozoe, T. Okamoto and S. W. Churchill, Natural convection in a vertical annular space heated from below. *Kagaku Kogaku Ronbunshu* **5,** 457–463 (1979). English translation — Heat Transfer — Japanese Research **8,** 82–93 (1979).
5. P. L. Silveston, Wärmedurchgang in waagerechten Flüssigkeitsschichten, *Forsch. Ing. Wes.* **24,** 59–69 (1958).
6. H. Ozoe, T. Okamoto, S. W. Churchill and H. Sayama, Natural convection in doubly inclined rectangular boxes, *Proceedings of the Sixth International Heat Transfer Conference.* Toronto, Canada, NC-19, **2,** 293–298 (1978).
7. P. L. T. Brian, A finite difference method of high-order accuracy for the solution of three-dimensional transient heat conduction, *A. I. Ch. E. Jl* **7,** 367–370 (1961).
8. M. R. Samuels and S. W. Churchill, Stability of a fluid in a rectangular region heated from below. *A. I. Ch. E. Jl* **13,** 77–85 (1967).
9. H. Ozoe, H. Sayama and S. W. Churchill, Natural convection in an inclined rectangular channel at various aspect ratios and angles — Experimental measurements. *Int. J. Heat Mass Transfer* **18,** 1425–1431 (1975).
10. H. Ozoe, S. W. Churchill, T. Okamoto and H. Sayama, Three-dimensional natural convection in inclined rectangular enclosures, *Proceedings of the Second Pacific Chemical Engineering Congress* **1,** 24–31 (1977).

CONVECTION NATURELLE DANS UN ESPACE ANNULAIRE INCLINE CHAUFFE ET REFROIDI A SES EXTREMITES PLANES

Résumé—On étudie expérimentalement et théoriquement la convection naturelle dans un espace annulaire chauffe et refroidi à ses extrémités planes et isole thermiquement aux parois latérales concentriques. Lorsque la surface chaude est inclinée depuis la position horizontale inférieure jusqu'à la position horizontale supérieure, le nombre de Nusselt moyen décroît tout d'abord, puis croît et décroît finalement jusqu'à l'unité, tandis que le mode de mouvement passe d'un arrangement symétrique de rouleaux cellulaires à des rouleaux distordus et obliques et à une circulation unique. La configuration d'écoulement est décrite à partir d'un traitement numérique appliqué à un modèle tridimensionnel et aussi par des photographies.

FREIE KONVEKTION IN EINEM GENEIGTEN ZYLINDRISCHEN RINGSPALT, DER AN SEINEN ENDFLÄCHEN GEHEIZT UND GEKÜHLT WIRD

Zusammenfassung—In einem geneigten Ringspalt, der an den Endflächen geheizt und gekühlt wurde und an den konzentrischen Zylinderwänden thermisch isoliert war, wurde die freie Konvektion experimentell und theoretisch untersucht. Wenn die geheizte Endfläche von der unteren waagerechten Position in die obere waagerechte Position geschwenkt wird, verringert sich zunächst die mittlere Nusselt-Zahl, dann erhöht sie sich und geht schließlich auf eins zurück, analog zur Art der Zirkulation, die von einer symmetrischen Rollzellenanordnung über verzerrte und schiefe Rollzellen zu einer Einzelzirkulation übergeht. Das Strömungsbild wird durch numerische Berechnung der Streichlinien nach einem dreidimensionalen Modell und ebenfalls mit Hilfe von Fotografien dargestellt.

ЕСТЕСТВЕННАЯ КОНВЕКЦИЯ В НАКЛОННОМ КОЛЬЦЕВОМ ЦИЛИНДРИЧЕСКОМ ЗАЗОРЕ, НАГРЕВАЕМОМ И ОХЛАЖДАЕМОМ С ТОРЦЕВЫХ ПОВЕРХНОСТЕЙ

Аннотация — Проведено экспериментальное и теоретическое исследование естественной конвекции в наклонном кольцевом зазоре, нагреваемом и охлаждаемом с торцевых поверхностей. Стенки концентрических цилиндров, образующих зазор, теплоизолированы. По мере перемещения нагреваемой поверхности с нижнего в верхнее горизонтальное положение среднее значение числа Нуссельта сначала уменьшается, затем увеличивается и, наконец, снижается до единицы в соответствии с тем, как изменяется режим движения от ряда симметричных круговых ячеек к искаженным и скошенным валообразным ячейкам и, наконец, к одноячейковой циркуляции. Картина течения представлена линиями тока, рассчитанными численно с помощью трехмерной модели, а также иллюстрируется фотографиями.